Experimental Gibbs Free Energy Considerations in the Nucleation and Growth of Single-Walled Carbon Nanotubes

Larry M. Wagg,* G. Louis Hornyak,† Leonid Grigorian,‡ Anne C. Dillon, Kim M. Jones, Jeffrey Blackburn, Philip A. Parilla, and Michael J. Heben*

National Renewable Energy Laboratory, Nanostructured Materials Research Group, 1617 Cole Blvd., Golden, Colorado 80401, Department of Physics and Astronomy, University of Denver, 2199 South University Blvd., Denver, Colorado 80208, and Honda Research Institute USA, 1381 Kinnear Rd., Ste. 116, Columbus, Ohio 43212

Received: January 25, 2005; In Final Form: April 4, 2005

Gas feed composition and reaction temperature were varied to identify the thermodynamic threshold conditions for the nucleation and growth of SWNT from methane on supported Fe/Mo catalyst. These reaction conditions closely approximate the pseudoequilibrium conditions that lead to the nucleation and growth of SWNT. These measurements also serve to determine an upper limit of the Gibbs free energy of formation for SWNT. The Gibbs free energy of formation relative to graphite is in good agreement with literature values predicted from simulations for SWNT nuclei containing approximately 80 atoms, while considerably larger than that predicted for bulk (5,5) SWNT. Our estimate over the range 700 to 1000 °C of 16.1 to 13.9 kJ mol^{-1} falls between the results of these simulations and literature values for diamond.

Introduction

Single-walled carbon nanotubes (SWNT) have been synthesized by a variety of techniques including electric-arc evaporation of graphite/metal mixtures,[1,2] laser vaporization of carbon/metal targets,[3] and chemical vapor deposition (CVD) with a wide variety of gaseous carbon sources.[4−7] While growth mechanisms for single-walled and multiwalled carbon nanotubes (MWNT) remain widely debated in the literature, little is known of the thermodynamics of the growth processes. Since laser vaporization and arc evaporation synthesis methods operate very far from equilibrium, CVD synthesis offers the best opportunity to study the formation energetics experimentally.

In a previous article we reported experimental parameters for efficient CVD growth of SWNT.[7] In the current work, we control the reaction parameters (temperature and reacting gas partial pressures) to provide increasing excess driving force relative to the equilibrium conditions expected for the methane/hydrogen/graphite system based on tabulated Gibbs free energy data.[8] The conditions that lead to the first appearance of SWNT are identified, and the Gibbs free energy of this nucleation threshold is calculated at various temperatures from the reaction parameters.

Experimental Details

Our SWNT CVD synthesis procedure was reported previously[7] and will not be presented in great detail here. Iron and molybdenum salts (6:1 Fe:Mo ratio, $Fe(SO_4)_2 \cdot 5H_2O$ (Aldrich, 97%) and $(NH_4)_6Mo_7O_{24} \cdot 4H_2O$ (Aldrich 99.98%)) were precipitated from an aqueous solution onto a slurry of high-surface-area fumed alumina support (Degussa Aluminumoxid C) in a manner similar to that reported by Cassell et al.[9] The supported catalyst was dried and ground to a fine powder. Approximately 100 mg of supported catalyst was distributed over ∼4 cm^2 on a quartz boat and placed in the middle of a 38 mm diameter quartz tube in a 35 cm, single zone, 800 W Lindberg/Blue M Mini Mite tube furnace. The bottom of the quartz boat was cylindrically curved to ensure good thermal contact with the interior of the quartz reactor tube. It is important to note that carbon decomposition only occurred on the supported catalyst, and self-decomposition of methane, or decomposition of methane on the tube walls or boat, was not observed.

The catalyst was oxidized in flowing zero grade air (all gases supplied by General Air) for 1 h at 850 °C, then reduced for 1 h at 600 °C under flowing argon/hydrogen mixture (90%/10%). The growth reaction was carried out immediately after the reduction step without exposing the reduced catalyst to ambient air. SWNT growth temperatures ranged from 600 to 1000 °C. The methane mole fraction in the feed gas was maintained at or below 10%, while the hydrogen mole fraction was varied from 0 to 99.5%. The gas feed was diluted with argon (99.999%) as required to maintain a total flow rate of 454 sccm, and absolute pressure was controlled at 600 Torr. A quadrupole mass spectrometer residual gas analyzer (Stanford Research Systems model RGA-100) was fitted to the reactor outlet to monitor gas concentrations in the reactor effluent.

The horizontal tube furnace temperature was controlled with use of a k-type thermocouple in contact with the outer surface of the quartz tube at the center of the 30 cm heated zone of the furnace. A second k-type thermocouple was inserted along the axis of the tube and positioned <1 cm above the catalyst bed. The difference in temperature between the inner and outer thermocouples never exceeded 2 °C when the furnace temperature was not being ramped. The inner thermocouple was used to report the temperature data for each experiment.

Samples were analyzed for SWNT content with Raman spectroscopy and transmission electron microscopy. Raman

* Address correspondence to this author at the National Renewable Energy Laboratory. E-mail: lawrence_wagg@nrel.gov; Michael_Heben@nrel.gov.

† University of Denver.

‡ Honda Research Institute USA.

10.1021/jp050445f CCC: $30.25
Published on Web 04/29/2005

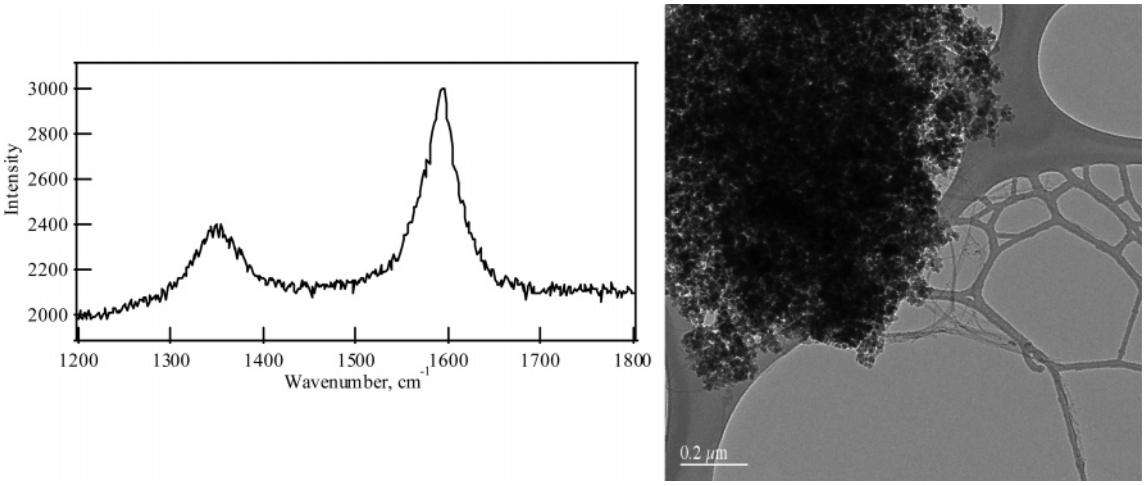

Figure 1. Raman spectrum (488 nm) and TEM image for first observation of SWNT nucleation (700 °C, 35% hydrogen, 10% methane, 55% argon). SWNT are visible in the lower right of the catalyst cluster.

spectroscopy was performed with the 2.54 eV (488 nm) line of an Ar ion laser and the 1.96 eV (632.8 nm) line of a HeNe laser. The backscattered light was analyzed with a Jobin Yvon 270M spectrometer equipped with a liquid nitrogen cooled Spectrum One CCD and a holographic notch filter. A Nikon 55 mm camera lens was employed both to focus the beam on the sample to a spot approximately 0.25 mm^2 in diameter and to collect the Raman scattered light. Averaging three 30-s scans was sufficient to obtain Raman spectra. Figure 1 shows Raman spectra and a TEM image for one SWNT nucleation threshold experiment.

Discussion

The thermodynamics of hydrocarbon decomposition over transition metal catalysts has been studied extensively by the petroleum refining community, which is interested in the suppression of coking reactions that lead to the deactivation of cracking catalysts.[10,11] The dominant coke forming reaction in these steam reforming systems produces filamentous carbon,[12] a broad group of fibril structures comprised mainly of stacked conical sheets of graphite. In rare cases, observed as early as 1971,[13,14] the planes of the graphite sheets were parallel to the axis of the filament, forming the structures known today as MWNT.

In 1945, Dent et al.[15] showed that the gas-phase composition of systems depositing carbon on transition metal catalysts deviated significantly from the equilibrium values predicted for the reaction forming graphite (C_g):

$$CH_4 \rightleftarrows C_g + 2H_2 \tag{1}$$

With the advent of the electron microscope in the early 1950s, the filamentous nature of the carbon structures was discovered.[12] In 1972, Rostrup-Nielsen[16] proposed that Dent had been measuring the equilibrium conditions for the reaction that forms filamentous carbon (C_{fc}):

$$CH_4 \rightleftarrows C_{fc} + 2H_2 \tag{2}$$

Through a series of experiments in which temperature and gas compositions were varied to drive either the forward (carbon deposition) or reverse (carbon etching) reactions, Rostrup-Nielsen measured the equilibrium gas compositions at various temperatures. From these data the temperature dependence of the equilibrium constant K_{fc} for filamentous carbon was determined. The Gibbs free energy of formation for filamentous carbon ΔG_{fc} could then be straightforwardly evaluated

$$\Delta G_{fc}(T) = -RT \ln[K_{fc}(T)] \tag{3}$$

where the equilibrium constant K_{fc} is calculated from gas partial

$$K_{fc}(T) = \left[\frac{P_{H_2}{}^2 a_c}{P_{CH_4}}\right] \tag{4}$$

pressures P_{H_2} and P_{CH_4}, and a_c, is the activity of carbon (unity for pure graphite). The same author presented similar results for the growth of MWNT with several collaborators in 1994.[17]

In this work, we use a method similar to Rostrup-Neilsen's to study the formation of SWNTs by determining the SWNT growth threshold constant, K^*_{SWNT}. This terminology follows the convention of Wagner and Froment,[18] who introduced the term coking threshold and its corresponding equilibrium constant, K^*_{fc}. The coking threshold constant was differentiated from the true equilibrium constant, K_{fc}, if the reaction sequence includes thermodynamically irreversible steps that prohibit observation of the true equilibrium conditions. Using the SWNT growth threshold constant, we may determine an upper bound for the Gibbs free energy of formation for SWNTs

$$\Delta G^*_{SWNT}(T) = -RT \ln[K^*_{SWNT}(T)] = -RT \ln\left[\frac{P_{H_2}{}^2}{P_{CH_4}}\right] \tag{5}$$

To facilitate discussion of our experimental results, we must define a new variable $\Delta G'(T)$, the Gibbs free energy driving force. This quantity is calculated from the gas partial pressures and the temperature employed in each experimental run designed to probe for SWNT growth (as in eq 5). The SWNT growth threshold $\Delta G^*(T)$ is that subset of $\Delta G'(T)$ where SWNT is first observed for a given gas mixture; SWNT are only observed in experiments where $\Delta G'(T)$ exceeds the threshold $\Delta G^*(T)$.

To access the critical thermodynamic information, we found it necessary to carefully consider the reaction when designing the experiments. Since the forward reaction yields two moles of hydrogen for every mole of methane consumed, examination of eq 5 reveals that if P_{H_2}:P_{CH_4} is held constant but the *total* pressure of these gases is varied (as when they are first introduced to the reactor) the driving force will vary with $\ln(1/P_{H_2})$. Figure 2a shows the effect on the driving force, $\Delta G'$,

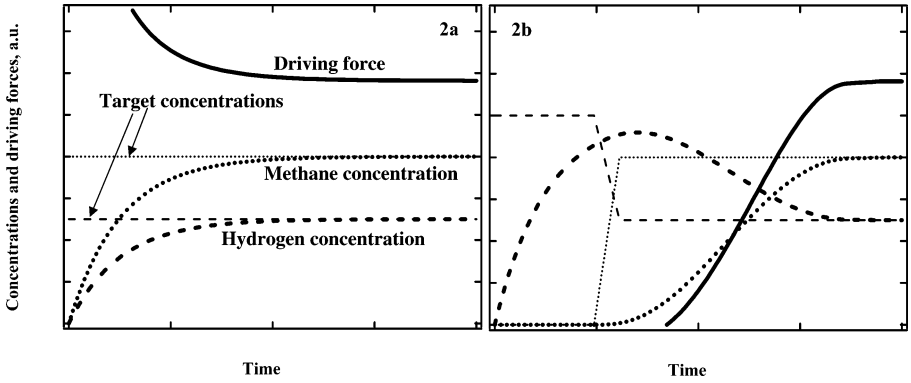

Figure 2. Gas concentration models and SWNT nucleation driving force $\Delta G'$. In part a, hydrogen (dashed lines) and methane (dotted lines) are admitted simultaneously. Concentration at the catalyst surface approaches the inlet concentration exponentially. $\Delta G'$ (solid line) declines from infinity to the desired target. In part b, an excess of hydrogen is admitted first, and after a delay methane is admitted gradually. $\Delta G'$ never exceeds the desired target.

if such a strategy is employed. A simple time dependent exponential model is used to calculate the gas concentration at the catalyst surface. The model shows that the driving force is initially infinite (when the reacting gases first arrive at the catalyst surface and $P_{H_2} \approx 0$), and then declines to the desired target as concentrations approach steady state. This brief period of elevated driving force may allow the nucleation of SWNT even though the eventual steady-state driving force may be insufficient to allow nucleation.

Figure 2b shows the alternative strategy used in this research. An excess of hydrogen is initially introduced to the reactor. After a short delay (typically 5 min), the control algorithm ramps the methane flow from zero to the experiment target, while at the same time decreasing hydrogen flow. With this approach the reaction driving force never exceeds the target value. Increments in $\Delta G'$ for each series of experiments (constant gas composition, varying only temperature) range from 0.2 to 0.4 kJ mol^{-1}.

The two different gas mixing schemes were compared by conducting two experiments with identical target conditions just below the threshold for SWNT growth, but employing the different strategies shown in Figure 2. Admitting the gases simultaneously as in Figure 2a led to the growth of SWNT, while no carbon deposition was observed with the scheme shown in Figure 2b.

Before beginning a detailed discussion of the data, it is necessary to consider whether the intended gas compositions and temperatures are actually obtained at the catalyst bed. Bulk isothermal conditions are confirmed by the use of two thermocouples. Oven temperature is controlled by using one thermocouple in external contact with the reactor tube, immediately below the catalyst boat in the center of the heated zone. The second thermocouple is inserted axially in the reactor, with the junction suspended approximately 1 cm immediately above the catalyst. While these thermocouples show a small offset (~10 °C) while the reactor is being heated, carbon deposition is not initiated until the axial thermocouple reaches the desired reaction temperature. During carbon deposition the two thermocouples never differ by more than 2 °C. Heat capacity calculations show that the reaction gases require approximately 9 W to be heated from room temperature to the reaction temperature, ~1% of the total furnace capacity.

Gas concentration profiles may be modeled by using mass balance differential equations and appropriate boundary conditions.[19] Using the information in Table 1, we consider the premixing of gases in the flexible corrugated stainless steel hose (1.5 m long) that connects the gas inlet manifold to the reactor.

TABLE 1: Experimental Parameters Relevant to Heat and Mass Transfer Calculations[a]

	feed line to reactor inlet	reactor hot zone
total gas flow, sccm	454	454
total gas concn, mol cm^{-3}	3.28×10^{-5}	8.49×10^{-6}
temp, K	293	1133
diffusion coeff,[19] cm^2 s^{-1}	0.726	10.55
tube diameter, cm	0.483	3.6
tube length, cm	150	15
residence time τ, s	2.67	3.8
av velocity, cm s^{-1}	56	3.9
viscosity,[36] μP	90	221
Reynolds no.	33	1.8
mixture heat capacity Cp,[37] J mol^{-1} K^{-1}	29.3	36.0
gas-phase heat transfer coeff k,[38] W m^{-1} K^{-1}		0.47
fused quartz heat transfer coeff k,[38] W m^{-1} K^{-1}		1.38

[a] Reaction parameters and physical properties of reactants: reaction temperature, 860 °C; mole fraction of methane, 0.1; mole fraction of hydrogen, 0.9; $\Delta G^*_{SWNT}(T)$, −17.48 kJ mol^{-1}.

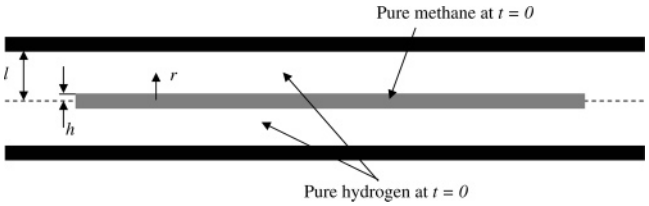

Figure 3. Initial boundary conditions for gas diffusion modeling. Pure methane and hydrogen strata are confined between two infinite flat plates.

Mixing in the laminar flow (Reynolds no. = 33) may be modeled considering the worst case scenario where hydrogen and methane are introduced as strata of pure gas, and mixing is due to diffusion alone. Figure 3 shows the geometry for a layer of pure methane located at the centerline between two infinite flat plates, with pure hydrogen occupying the remainder of the space. The time-dependent concentration profile in such a system has been solved by Barrer,[20]

$$C = C_o\left[\frac{h}{l} + \frac{2}{\pi}\sum_{n=1}^{\infty}\sin\left(\frac{n\pi h}{l}\right)\exp\left(\frac{-D_{CH_4-H_2}n^2\pi^2 t}{l^2}\right)\cos\left(\frac{n\pi r}{l}\right)\right] \quad (6)$$

where C_0 is the initial concentration from $0 < r < h$, and

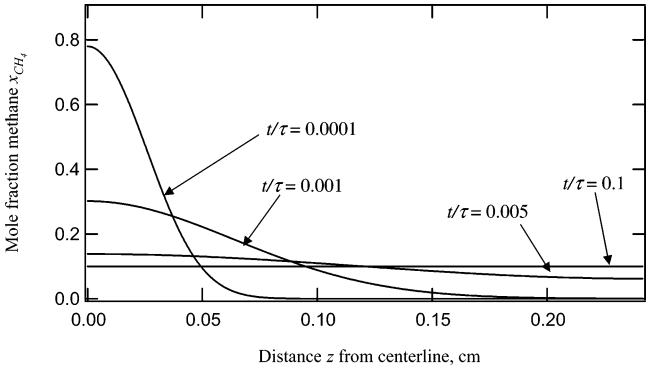

Figure 4. Evolution of methane concentration profile between two infinite flat plates.

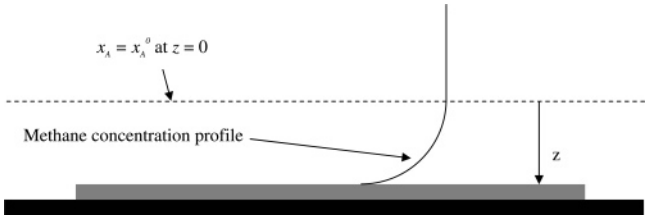

Figure 5. Stagnant diffusion layer model used to calculate depletion of methane at catalyst surface.

$D_{CH_4-H_2}$ is the bimolecular diffusion coefficient. Figure 4 shows the dependence of concentration on position r between the plates for various values of t/τ, where τ is the average time required for the gas to move from the manifold to the reactor (~2.7 s). The calculation shows that diffusion alone produces rapid mixing in this small diameter tube such that concentration gradients are negligible (<0.1% variation) at $t/\tau = 0.1$. While this simple model differs from the cylindrical geometry in the actual experiment, it is clear that the gases entering the reactor will be adequately mixed. The concentration gradient is linearly dependent on the flux in the planar system and dependent on the *square root* of the flux in the cylindrical system, but this difference cannot reduce mixing efficiency by more than an order of magnitude as would be required to compromise mixing.

We must also consider the possibility that carbon deposition proceeds rapidly enough to deplete the methane concentration at the catalyst surface. We may model the system as shown in Figure 5, where the catalyst is separated from the bulk gas by a stagnant gas layer through which methane must diffuse. The solution to a mass balance in this system at steady state is

$$\frac{N_{CH_4} z}{c D_{CH_2-H_2}} = \ln\left(\frac{1 + x_{CH_4}^0}{1 + x_{CH_4}}\right) \quad (7)$$

where c is the total gas concentration, N_{CH_4} is the molar methane flux, x_{CH_4} is the methane mole fraction at position z, and $x_{CH_4}^0$ is the bulk methane mole fraction. The bimolecular diffusion coefficient at a typical reaction temperature (860 °C) may be estimated to be 10.5 $cm^2\ s^{-1} \pm 8\%$.[19] Average carbon flux may be calculated from the mass of carbon deposited, which ranges from 1 to 4 mg for the catalyst bed of approximately 4 cm^2. Using 4 mg, the maximum mass deposited in any SWNT nucleation threshold experiment, we may then estimate the thickness of the diffusion layer z that would lead to a depletion of 1% in the methane concentration at the catalyst surface ($x_{CH_4}(z) = 0.99 x_{CH_4}^0$). This distance turns out to be 3.5 cm, nearly the entire diameter of the reactor. Since the laminar flow of gases across the top of the boat will restrict the actual boundary layer thickness to less than 1 cm, it is apparent that diffusion is sufficient to maintain methane concentration deviation from bulk concentration to less than 1%. While the reaction is expected to proceed at a significantly faster rate when methane is first admitted to the reactor, the rate will then drop quickly below the average rate calculated above, at which time the methane concentration deviation will be ≪1%.

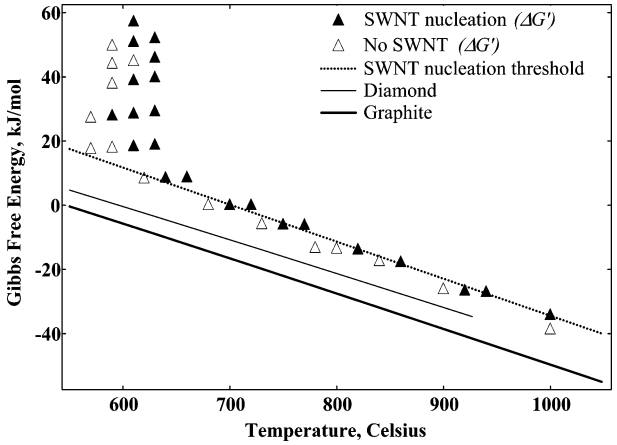

Figure 6. Gibbs free energy and the SWNT nucleation threshold. Symbols represent individual experiments with calculated driving force $\Delta G'$. Experiments in the highly activated region (<700 °C) range are not included when determining the growth threshold. The dotted line is a regression fit to those experiments showing first indication of SWNT nucleation for each gas composition. Experimental parameters for these ΔG^*_{SWNT} threshold experiments are shown in Table 2. Literature values for ΔG_f for graphite and diamond are also included in this graph (solid lines).

The average reaction rate also allows us to calculate the rate at which heat is absorbed by the endothermic reaction. The average heat flux is 7 mW, less than 2 mW/cm^2 over the 4 cm^2 catalyst bed. Even neglecting any heat transfer from the gas phase, conduction through the quartz boat is sufficient to maintain the average reaction rate with a temperature differential of 2.5 °C. As for the diffusion discussion above, the initial rate will be faster than the average and so any temperature differential will quickly become negligible. Note that it is sufficient for our purposes that our target levels are realized *at any time* within the duration of the carbon deposition cycle since we seek only the conditions for the first occurrence of SWNT nucleation.

In summation, the experimental design employed here is very different from the one analyzed by Grujicic et al.,[21] and is not subject to inhomogeneous reactant or temperature distributions. These authors base their work on the experiments of Ruckenstein and Hu,[22] who report deposition rates 2 orders of magnitude greater than those observed in our experiments when methane flow rates are normalized.

In Figure 6 we have plotted the calculated Gibbs free energy driving force $\Delta G'$ as a function of temperature for the series of experiments. Experimental parameters for the SWNT nucleation threshold reactions are shown in Table 2. Gas compositions ranged from 10% CH_4/10% H_2/80% Ar at 570 °C to 0.5% CH_4/99.5% H_2/0% Ar at 1000 °C. Literature $\Delta G(T)$ functions for graphite and diamond are also included.[8] Sets of experiments with the same gas composition follow nearly horizontal lines with a slight slope; 14 different compositions and a total of 37 experiments are shown in this plot. The presence of SWNT in the samples was confirmed by Raman spectroscopy (λ = 488 and 632 nm) and TEM imaging. No MWNT or double-wall carbon nanotubes were observed in any samples imaged.

TABLE 2: Reaction Parameters for Experiments Which Identified the SWNT Nucleation Threshold

mole fraction of hydrogen	mole fraction of methane	temp, °C	ΔG^*_{SWNT}, kJ mol^{-1} K^{-1}
35	10	700	0.27
50	10	750	−5.7
75	10	820	−13.5
90	10	860	−17.4
95	5	920	−26.3
97	3	1000	−33.9

The experimental results in Figure 6 may be divided into two distinct regions. Below approximately 630 °C, SWNT do not nucleate unless the driving force $\Delta G'$ is significantly above the straight line that describes the temperature dependence of the SWNT growth threshold ΔG^* at temperatures above 700 °C. Thus the reaction appears to be strongly thermally activated in this low-temperature region, and no SWNT growth is observed below 590 °C. SWNT yield was very low in this activated region, with significant quantities of other carbon species (graphite and amorphous carbon) making positive identification of SWNT difficult. Above 700 °C, the driving force for the SWNT growth threshold is a linear function of temperature. A regression fit ($R^2 = 0.9986$) leads to the expression

$$\Delta G^*(T) = -0.116T + 80.96 \text{ kJ/mol}, \quad 720\ ^\circ\text{C} < T < 1000\ ^\circ\text{C} \quad (8)$$

In Rostrup-Nielsen's original work,[16] ΔG^* was interpreted as the Gibbs free energy of formation for carbon filaments. However, as mechanistic models for carbon filament growth were developed over the next several years, it became apparent that this work had measured the pseudoequilibrium conditions associated with an intermediate species rather than with the filaments themselves.[23] Extensive evidence shows that in the filamentous carbon system, as the carbon source gas decomposes at the catalyst surface, a layer of metastable carbide or carbide-like structure forms. Carbon from the carbide layer dissolves into the bulk catalyst metal below, diffusing through the metal catalyst particle, and is rejected from the metal at the interface between the metal and the catalyst support. Thus carbon filaments nucleate between the catalyst particle and the support, and lift the catalyst particle off the support as the filaments grow.[24] This mechanism, known as the tip growth model, is believed to be responsible for the growth of both filaments[25] and MWNT[26] since TEM images have shown these structures to have metal catalyst particles embedded in their tips.

The carbon activity in the catalyst particle is not constant during this measurement and therefore the gas-phase carbon activity is only in pseudoequilibrium with the surface carbide structure rather than with the carbon filaments themselves. This led to the conclusion that Rostrup-Nielsen's work had measured the equilibrium conditions associated with the formation of an intermediate species (the surface carbide) rather than the carbon filaments.[27]

In contrast, SWNT are thought to grow primarily through the root growth mechanism, which begins with the formation of a curved carbon cap that detaches from the surface of a small catalyst particle and grows as carbon atoms diffuse across the surface of the catalyst and attach to the SWNT.[28] Since carbon atoms remain on the surface of the catalyst particle, the slow bulk diffusion step is eliminated. However, the growth mechanism is unlikely to be free of thermodynamically irreversible steps that can decouple the gas composition from equilibrating with SWNT. While the kinetics of methane decomposition over transition metal catalysts is still widely debated in the literature,[29]

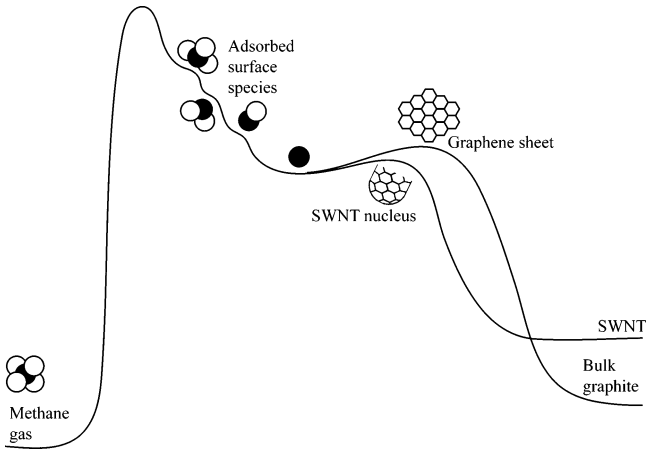

Figure 7. Reaction coordinate in the nucleation and growth of SWNT and bulk graphite.

the mechanism and rate controlling steps are generally accepted. Methane is first chemisorbed with the abstraction of a single hydrogen atom. This is thought to be the rate controlling step, and Zein recently reported activation energy for this step of 60 kJ/mol,[30] while noting that previously reported literature values for the activation energy ranged from 90 to 236 kJ/mol.[31−33] Subsequent hydrogen abstractions are fast, such that the adsorbed, fully dehydrogenated carbon atom (C*) is the most abundant carbon surface species.[29]

The knitting of carbon species to form SWNT and graphitic structures has been studied primarily through computer simulations,[30,34,35] and Fan et al. recently reported detailed calculations of the energetics of the nucleation of SWNT and graphene sheets.[35] Nucleation of SWNT and addition of carbon atoms to the base of a growing tube were determined to be very fast and thermodynamically irreversible,[30] and it may be at this point that the carbon atoms are decoupled from the gas-phase carbon activity.

Figure 7 shows our proposed model of the reaction coordinate and intermediates involved in the nucleation and growth of SWNT. Initially we consider the case where the driving force is very low. Methane molecules cross the initial activation barrier as the first hydrogen atom is abstracted, and the removal of the remaining hydrogen atoms is fast, leaving adsorbed carbon atoms as the dominant carbon-containing species. High hydrogen concentrations drive the reverse reaction and keep surface carbon concentrations low.

As the driving force is increased, the population of surface carbon atoms increases. These begin to coalesce, and eventually overcome the second, smaller activation barrier to nucleate either SWNT or graphene sheets. Under the reaction conditions employed in these experiments, the SWNT nucleus is energetically favored relative to graphene because the curved structure allows edge atoms to remain adsorbed, reducing the number of high-energy dangling bonds.[35]

After nucleation, the carbon structures act as a sink for surface carbon atoms, and this depletion perturbs the equilibrium with the gas phase by inhibiting the re-formation of methane, thereby enhancing the net forward methane decomposition reaction. While the highly energetic carbon atoms are free to add to the structure, contact with the gas-phase methane activity is not maintained through this relaxation. Therefore, ΔG^* is a measure of the Gibbs free energy of formation of these surface species and represents an upper limit for $\Delta G_f(T)$ of bulk SWNT.

These observations suggest that the strategy of introducing the reacting gases simultaneously may in fact be an excellent

way to maximize the growth of long, low defect SWNT. During the induction period of elevated driving force, many SWNT will nucleate. But as concentrations approach steady state, the driving force is decreased. A window of driving force should exist that is not great enough to overcome the second activation barrier and nucleate new SWNT, but would still provide carbon for the continued growth of existing tubes. This would simultaneously maintain catalyst surface area free from SWNT and slow the rate of growth of existing tubes such that they would be able to approach their minimum energy state without defects.

It is inappropriate to compare our results to those for MWNT reported by Tavares et al.[17] due to the differences in the root (SWNT) and tip (MWNT) growth models. That study found $\Delta G^*_{\mathrm{MWNT}}$ values ranging from 4.5 to 15 kJ/mol for the disproportionation of carbon monoxide over nickel/copper catalysts at 873 K, and this is most appropriate to compare to the $\Delta G_f(T)$ of iron carbide (approximately 5.3 kJ/mol at 873 K) since the metastable carbide layer in the tip growth model is the disconnect between gas phase and bulk solid carbon activities.[27]

We are left then to compare with the results of simulations at 723 °C by Fan et al.,[35] who calculated that the total energy of 85 atoms forming a SWNT nucleus (40 atom cap and 45 atom tube) was 17.3 eV, equivalent to 20.2 kJ/mol relative to graphite. This compares favorably with our experimental values of 15.6 kJ/mol calculated with eq 5. The calculated energy for an infinite (5,5) tube (a small diameter; CVD tubes are more typically (10,10) or similar) in this same reference is 6.7 kJ/mol, considerably smaller than our experimental value and quite similar to that of diamond at the same temperature (6.0 kJ/mol).

In conclusion, we have determined the pseudoequilibrium conditions that characterize SWNT nucleation and growth from methane on supported metal catalysts. The results define an upper bound for the Gibbs free energy of formation $\Delta G_f(T)$ for bulk SWNT, but may more accurately describe the formation of an intermediate species such as chemisorbed carbon atoms. Our experimentally determined value is smaller than that recently calculated for SWNT nucleii by Fan et al.,[35] and greater than calculated values for bulk SWNT.

Acknowledgment. The authors acknowledge support for this project from the Office of Science, Basic Energy Sciences, Division of Materials Science and the Office of Energy Efficiency and Renewable Energy Hydrogen, Fuel Cell, and Infrastructure Technologies Program of the Department of Energy under Grant No. DE-AC36-99GO10337. L.M.W. thanks Robert L. McCormick of NREL and John E. Shilling of the University of Colorado (Department of Chemistry) for helpful discussions.

References and Notes

(1) Iijima, S.; Ichihashi, T. *Nature* **1993**, *363*, 603.
(2) Bethune, D. S.; Kiang, C.-H.; Vries, M. S. d.; Gorman, G.; Savoy, R.; Vasquez, J.; Beyers, R. *Nature* **1993**, *363*, 605.
(3) Guo, T.; Nikolaev, P.; Thess, A.; Colbert, D. T.; Smalley, R. E. *Chem. Phys. Lett.* **1995**, *243*, 49.
(4) Dai, H.; Rinzler, A. G.; Nikolaev, P.; Thess, A.; Colbert, D. T.; Smalley, R. E. *Chem. Phys. Lett.* **1996**, *260*, 471.
(5) Peigney, A.; Laurent, C.; Dobigeon, F.; Rousset, A. *J. Mater. Res.* **1997**, *12*, 3.
(6) Hafner, J. H.; Bronikowski, M. J.; Azamian, B. R.; Nikolaev, P.; Rinzler, A. G.; Colbert, D. T.; Smith, K. A.; Smalley, R. E. *Chem. Phys. Lett.* **1998**, *296*, 195.
(7) Hornyak, G. L.; Grigorian, L.; Dillon, A. C.; Parilla, P. A.; Jones, K. M.; Heben, M. J. *J. Phys. Chem. B* **2002**, *106*, 2821.
(8) *NIST-JANAF Thermochemical Tables*, 4th ed.; Chase, M. W. J., Ed. *J. Phys. Chem. Ref. Data* **1998**.
(9) Cassell, A. M.; Raymakers, J. A.; Kong, J.; Dai, H. *J. Phys. Chem. B* **1999**, *103*, 6484.
(10) Bartholomew, C. H. *Catal. Rev.*: *Sci. Eng.* **1982**, *24*, 67.
(11) Trimm, D. L. *Catal. Rev.*: *Sci. Eng.* **1977**, *16*, 155.
(12) Kehrer, V. J.; Leidheiser, H. J. *J. Phys. Chem.* **1954**, *58*, 550.
(13) Robertson, S. D. *Carbon* **1971**, *8*, 365.
(14) Baird, T.; Fryer, J. R.; Grant, B. *Nature* **1971**, *233*, 329.
(15) Dent, F. J.; Cobb, J. W. *Trans. Inst. Gas Eng.* **1945**, 602.
(16) Rostrup-Nielsen, J. R. *J. Catal.* **1972**, *27*, 343.
(17) Tavares, M. T.; Alstrup, I.; Bernardo, C. A.; Rostrup-Nielsen, J. R. *J. Catal.* **1994**, *147*, 525.
(18) Wagner, E. S.; Froment, G. F. *Hydrocarbon Proc.* **1992**, *71*, 69.
(19) Bird, R. B.; Stewart, W. E.; Lightfoot, E. N. *Transport Phenomena*; Wiley: New York, 1960.
(20) Barrer, R. M. *Diffusion in and through solids*; Cambridge University Press: New York, 1951.
(21) Grujicic, M.; Cao, G.; Gersten, B. *J. Mater. Res.* **2003**, *38*, 1819.
(22) Ruckenstein, E.; Hu, Y. H. *Carbon* **1998**, *36*, 269.
(23) Bianchi, E. C.; Lund, C. R. F. *J. Catal.* **1989**, *117*, 455.
(24) Alstrup, I. *J. Catal.* **1988**, *109*, 241.
(25) Snoeck, J. W.; Froment, G. F.; Fowles, M. *J. Catal.* **1997**, *169*, 240.
(26) Nolan, P. E.; Lynch, D. C.; Cutler, A. H. *J. Phys. Chem. B* **1998**, *102*, 4165.
(27) DeBokx, P. K.; Kock, A. J. H. M.; Boellaard, E.; Klop, W.; Geus, J. W. *J. Catal.* **1985**, *96*, 454.
(28) Terrones, H.; Terrones, M.; Hernandez, E.; Grobert, N.; Charlier, J.-C.; Ajayan, P. M. *Phys. Rev. Lett.* **2000**, *84*, 1716.
(29) Wei, J.; Iglesia, E. *J. Phys. Chem. B* **2004**, *108*, 4094.
(30) Zein, S. H. S.; Mohamed, A. R.; Sai, P. S. T. *J. Am. Chem. Soc.* **2004**, *43*, 4864.
(31) Alstrup, I.; Tavares, M. T. *J. Catal.* **1993**, *139*, 513.
(32) Kuvshinov, G. G.; Mogilnykh, Y. I.; Kuvshinov, D. G. *Catal. Today* **1998**, *42*, 357.
(33) Muradov, N. *Proceedings of the 2000 hydrogen program review*; U.S. Department of Energy: Washington, DC, 2000.
(34) Ding, F.; Bolton, K.; Rosen, A. *J. Phys. Chem. B* **2004**, *108*, 17369.
(35) Fan, X.; Buczko, R.; Puretzky, A.; Geohegan, D.; Howe, J. Y.; Pantelides, S. T.; Pennycook, S. J. *Phys. Rev. Lett.* **2004**, *90*, 145501.
(36) Reid, R. C.; Prausnitz, J. M.; Sherwood, T. K. *The Properties of Gases and Liquids*; McGraw-Hill: New York, 1958.
(37) *CRC Handbook of Chemstry and Physics*, 62 ed.; Weast, R. C., Astle, M. J., Eds.; CRC Press: Boca Raton, FL, 1981.
(38) Hirschfelder, J. O.; Curtiss, C. F.; Bird, R. B. *Molecular theory of gases and liquids*; Wiley: New York, 1954.